Continental Shelf Research 214 (2021) 104327

Contents lists available at ScienceDirect

Continental Shelf Research

journal homepage: http://www.elsevier.com/locate/csr

Rapid organic matter cycling in North Sea sediments

Emil De Borger [a,b,*], Ulrike Braeckman [a], Karline Soetaert [b,a]

[a] Ghent University, Department of Biology, Marine Biology Research Group, Krijgslaan 281/S8, 9000, Ghent, Belgium
[b] Royal Netherlands Institute of Sea Research (NIOZ), Department of Estuarine and Delta Systems, and Utrecht University, Korringaweg 7, P.O. Box 140, 4401, NT, Yerseke, the Netherlands

ARTICLE INFO

Keywords:
Diagenetic modelling
Sediment biogeochemistry
Nutrient exchange
North sea
Shelf sea

ABSTRACT

Coastal shelf seas are zones of intense nutrient cycling, where a strong coupling between the sediment and the water column enhances primary productivity. To identify factors that control the strength of this benthic-pelagic coupling we measured sediment characteristics, solute fluxes, and porewater nutrient profiles in spring along a south - north transect in the North Sea crossing distinct regions: the shallow Oyster Grounds closest to the Dutch shore, the shallow Dogger Bank, the 80-m deep central North Sea, and the 150-m deep Fladen Grounds between the north of Scotland and Norway. The data were used to constrain rates of different mineralization processes with the 1-D diagenetic model (OMEXDIA). Surprisingly, we found no major differences in the biogeochemical signature along the 670 km long North Sea transect, despite sediments ranging in median grainsize from 25 to 217 μm, and a permeability range >3 orders of magnitude. Total carbon mineralization ranged between 4 and 13.5 mmol C m^{-2} d^{-1}, and decreased significantly northward. Oxic mineralization was the dominant mineralization process in all studied sites. Finest, least permeable sediments were found in the Fladen Grounds where highest denitrification rates were recorded, linked to high nitrate concentrations in the overlying water. The coarsest, most permeable sediments of the shallow Dogger Bank represented a transition area between the Oyster Grounds, where oxic mineralization was highest (75–90%), and the central North Sea samples, where anoxic mineralization increased relative to oxic mineralization due to higher bioturbation rates (oxic: 59–72%, anoxic: 27–39%). Overall, denitrification rates increased, while phosphorus removal tended to decrease northward. This contrasting behaviour in nitrogen and phosphorus removal was identified as a possible cause for decreasing DIN: DIP ratios in the water column towards the north.

1. Introduction

Every spring, when irradiance and temperatures increase in the surface waters of coastal seas in temperate and higher latitudes, inorganic carbon and free nutrients are captured as organic matter in vast algae blooms. Part of this organic matter settles on sediments, where it is remineralized into free nutrients by a set of chemical, physical, and biological processes, collected under the term “early diagenesis” (Boudreau, 2000). Shelf seas account for up to 80% of global benthic mineralization, despite covering only 7% of the seafloor (Wollast, 1998). More so, shelf sediments account for an estimated third of all nitrogen loss from the global ocean through denitrification (Middelburg et al., 1996) and for 50–84% of total phosphorus burial, making these regions crucial in the regulation of eutrophication (Galloway et al., 2004; Seitzinger et al., 2006; Slomp, 2011).

The North Sea is a shelf sea bordering the NE Atlantic, with a surface area of about 575 000 km^2, where shallow waters in the south (~ 40 m) make way for deeper waters towards the north (> 80 m). With the exception of the Norwegian trench (725 m), depths do not exceed 250 m (Fig. 1). Bordered by several industrialized nations, the North Sea receives considerable nutrient input through river discharge and, though on the decline, this input heavily affects nutrient levels in the coastal zone (Burson et al., 2016; Lenhart et al., 2010). Further offshore, nutrient levels are more regulated by input of Atlantic waters (Lenhart et al., 2010).

Organic matter deposition is strongly dependent on algae blooms, which are estimated to produce on average 180 g C m^{-2} y^{-1} of organic matter (van Leeuwen et al., 2013). The main phytoplankton bloom occurs in April–May, and is strongest in the nutrient rich, well mixed waters of the southern part of the North Sea, and along the eastern boundary (Fig. 1). In the more central and northern, stratified, regions of the North Sea, surface nutrients are rapidly consumed during the initial

* Corresponding author. Ghent University, Department of Biology, Marine Biology Research Group, Krijgslaan 281/S8, 9000, Ghent, Belgium.
E-mail address: emil.de.borger@nioz.nl (E. De Borger).

https://doi.org/10.1016/j.csr.2020.104327
Received 12 October 2020; Received in revised form 8 December 2020; Accepted 14 December 2020
Available online 23 December 2020

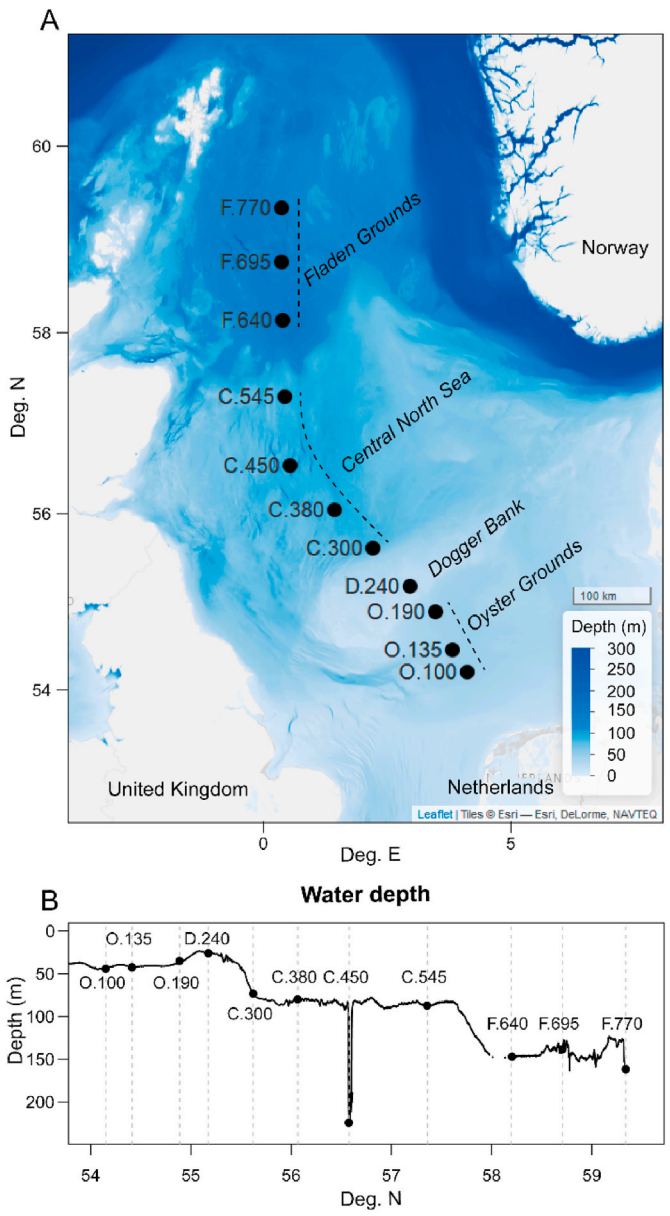

Fig. 1. (A) Stations sampled in the North Sea during the NICO 10 research campaign. (B) Water depth along the transect in latitudinal direction.

phytoplankton bloom, and are not replenished until autumn when waters get mixed again through advective overturning and storm events (Tijssen and Wetsteyn, 1984; Van Haren et al., 2003). A deep chlorophyll maximum (DCM) then forms near the thermocline, on the condition that this is within the euphotic zone. Here together with light, nutrients from the deeper, mixed water column are accessible to fuel primary productivity throughout the summer (Weston et al., 2005; van Leeuwen et al., 2013).

This primary production is predominantly deposited near the production sites, but it also gets transported through successive deposition-resuspension events (Van Raaphorst et al., 1998). The dominant counterclockwise residual currents transport fine-grained, organic matter rich material from the highly dynamic Southern Bight, along the eastern boundaries, towards the Skagerrak. As a consequence of this water circulation pattern, the reactivity, or "freshness" of deposited organic matter decreases towards the site of final deposition, the Skagerrak, relative to the initial production site (Dauwe and Middelburg, 1998). These patterns of deposition broadly correspond to the sediment composition. Recently published synthetic maps of several sediment-related variables (Wilson et al., 2018) highlighted the general shift in particle size when moving from the highly dynamic southern North Sea, where finer sediments are resuspended, towards the deeper northern North Sea.

The sediment composition and its resulting permeability (among others) regulate the magnitude of solute transport processes, the oxygen penetration depth, and the structure of microbial communities (Probandt et al., 2017; Ahmerkamp et al., 2020). In coarse grained sediments, organic matter is rapidly mineralized, because of the high availability of oxygen, the most efficient electron acceptor, penetrating deeply in the sediment matrix (Glud, 2008; Huettel et al., 2014). These sediments are characterized by relatively high oxygen consumption rates, but low stocks of organic carbon (Braeckman et al., 2014; Brenner et al., 2016). In fine-grained cohesive sediments on the other hand, organic matter is trapped between sediment grains, and oxygen penetrates mere millimetres, resulting in a higher proportion of anoxic mineralization and a build-up of organic carbon (Jørgensen, 1982; Canfield et al., 1993). At the same time, decomposition in the water column is expected to decrease the deposition of organic matter with increasing water depth (Brenner et al., 2016; Middelburg et al., 1997). Denitrification is also mainly regulated by organic matter deposition rates, with highest rates of denitrification expected where intermediate (4–9 mmol C m^{-2} d^{-1}) mineralization rates occur (Soetaert et al., 2000), as this combines an optimal balance between sufficiently low oxygen and sufficiently high nitrate availability, with sufficient carbon availability to allow mineralization to proceed (Cardenas et al., 2008).

In recent decades, phytoplankton blooms in the North Sea occur earlier in the year, and phytoplankton production has decreased notably in areas under riverine influence. While this is likely due to de-eutrophication, decreasing trends are also seen for areas further away from the coast (Capuzzo et al., 2018; Desmit et al., 2019). North Sea surface temperature (SST) has increased by 1.6 °C between 1971 and 2014, and warming of surface waters affects the stratified regions further away from shore such as the central North Sea, with declines in phytoplankton biomass as a result (Holt et al., 2016; Desmit et al., 2019).

Given this range of controls on mineralization processes, a thorough understanding is needed to anticipate future changes to benthic nutrient cycling, for example caused by decreased carbon inputs or human induced changes to sediment characteristics. However, the sediment biogeochemistry is poorly characterized for large areas of the North Sea, such as the central North Sea northwest of the Dogger Bank, or the Fladen Grounds, where only a handful of studies have reported measurements (Fig. 1; Upton et al., 1993; de Wilde et al., 1986; Brenner et al., 2016; Rosales Villa et al., 2019).

The aims of the study were to characterize the *in situ* response of regions with differing sedimentological characteristics to the deposition of fresh organic matter, and to isolate potential driving factors behind observed differences in biogeochemical functioning. Shipboard incubations of sediment cores were performed to derive solute fluxes, and porewater profiles were established. A diagenetic model was subsequently used to derive rates of organic matter mineralization processes.

2. Materials and methods

2.1. Study area

During the NICO-10 research expedition (Netherlands Initiative Changing Oceans, leg 10, May 25, 2018 - June 5, 2018) sediments were sampled from aboard the RV Pelagia at 11 stations along a 670 km long transect, from station "Oyster Grounds 100" (54.1494° N, 4.3419° E) near the Dutch coast, to station "Fladen Grounds 770" (59.4167° N, 0.4222° E) in the NW of the North Sea (Fig. 1, Table 1). In what follows, numbers in the station names indicate the distance travelled away from shore along the transect. This transect crossed multiple zones of interest:

Table 1
Sampling dates and locations of stations, and bottom water concentrations.

Station	Sampling dates, 2018	Latitude (Deg. N)	Longitude (Deg. E)	Depth (m)	PO_4^{3-} (mmol m^{-3})	NH_4^+ (mmol m^{-3})	NO_3^- (mmol m^{-3})	O_2 (mmol m^{-3})
O.100	June 5	54.14938	4.341914	45	0.6	3.0	1.5	230
O.135	June 4	54.41973	4.046748	43	0.4	1.5	0.9	253
O.190	June 3	54.87539	3.686554	41	1.0	5.7	3.6	281
D.240	May 25	55.17374	3.161264	26	0.3	6.8	0.7	290
C.300	June 2	55.62316	2.384164	72	0.7	4.4	1.1	201
C.380	June 1	56.06932	1.599237	79	1.3	5.7	3.7	255
C.450	May 26	56.58769	0.685672	224	1.1	32.8	5.2	294
C.545	May 31	57.36059	0.579088	84	1.1	5.4	5.5	253
F.640	May 27	58.20097	0.525871	148	1.8	6.0	11.1	251
F.695	May 29	58.83913	0.511693	135	1.5	6.0	8.5	248
F.770	May 30	59.41514	0.509838	135	3.1	3.8	8.8	237

the Oyster grounds (OG, sts. O.100, O.135, O.190), the Dogger Bank (D.240), the central area from the north of the Dogger Bank up to the deepest station, Devils Hole (sts. C.300, C.380, C.450, C.545), and the Fladen Grounds in the north (sts. F.640, F.695 and F.770). The Oyster Grounds is an area with maximal water depths of 50 m, with well mixed water in winter, and stratified conditions in summer (Greenwood et al., 2010). The Dogger Bank is a 260 km long shallow sand bank with water depths of 20–40 m. Northward from this area the seabed slopes down to a more or less constant depth of 80 m, except for the > 260 m deep depression called "Devils Hole". In this area and further northward, waters are stratified from spring onwards, with continuously mixed conditions in winter (van Leeuwen et al., 2015). Towards the Fladen Grounds there is a further increase in depth (100–150 m), where seasonal variations in temperature of these deeper bottom waters are small. Published estimates for primary productivity in these regions are fairly similar, and range between 100 and 250 g C m^{-2} y^{-1} on the Oyster Grounds (Gieskes and Kraay, 1984; Joint and Pomroy, 1993), 270 g C m^{-2} y^{-1} for a stratified site in the central North Sea (Weston et al., 2005), and 150–200 g C m^{-2} y^{-1} for the Northern North Sea (Reid et al., 1990).

2.2. On-board incubations

Sediments were sampled using a stainless steel NIOZ boxcorer (30 cm ID, 50 cm height), specially designed for on-board sediment measurements as the entire sediment sample can be incubated. At each location three intact boxcores were collected. The sediment surface in the boxcores was inspected for intactness, and subsequently covered with a Plexiglas lid with sampling ports and a built-in Teflon coated magnetic stirring motor that kept the overlying water homogenized. Bottom water (±5 m above the bottom) collected from NISKIN bottles was added to each boxcore to seal the sample airtight. The samples were then placed into large buffer tanks that maintained constant temperature (~bottom water temperature of 11 °C) and were kept in the dark to prevent photosynthetic activity. To determine the sediment oxygen consumption rates, the oxygen concentration in the water overlying the sediment was monitored (1 Hz) with optode sensors (FireStingO2, Pyroscience). A two-point calibration of the sensors was conducted prior to measurements, using 100 and 0% oxygen saturated seawater to represent water column and anoxic O_2 concentrations, respectively.

The samples were left to acclimatize for a period of 2 h, before starting nutrient flux measurements. Five water samples were collected for flux measurements over a period of 48 h. Nutrient samples were collected by extracting a volume of 50 mL from the overlying water, while simultaneously injecting the same amount of bottom water through a second sampling port to prevent air intrusion. Five mL of this volume was used for nutrients (ammonium (NH_4^+), nitrate (NO_3^-), phosphate (PO_4^{3-}), filtered through a 0.45 μm syringe filter), and 10 mL for dissolved inorganic carbon (DIC, 10 mL headspace vials). Nutrient samples were stored at −20 °C, DIC samples were poisoned with 1 μL of saturated $HgCl_2$ per mL sample for preservation, and placed into a 4 °C refrigerator. Upon thawing, nutrient samples were analysed in the lab, by a SEAL QuAAtro segmented flow analyser (Jodo et al., 1992). DIC analysis was performed using a segmented flow analyser (San++ SKALAR) following Stoll et al. (2001). Quality control of output from the flow analyzers is routinely performed with reference material from Osil and Quasimem (nutrients), and University of California San Diego (DIC).

Fluxes (in mmol m^{-2} d^{-1}) were calculated by fitting a linear regression through the concentration time series, and multiplying the regression coefficient by the height of the overlying water to convert from volumetric to surface standardized rates. If the regression was not significant (i.e. $p > 0.1$), the flux was interpreted as 'zero'. For oxygen fluxes the same method was applied to a consistently decreasing section of the oxygen concentration data.

At the end of the incubation period, several subsamples were collected from each boxcore to determine: sediment porosity and grainsize (2 cm of top sediment, Ø 2 cm), sediment organic carbon and nitrogen (2 cm of top sediment, Ø 2 cm), sediment permeability (~ 15 cm of sediment, Ø 3.6 cm), porewater nutrient profiles (~ 20 cm of sediment, Ø 10 cm Plexiglass sampling core), and oxygen microprofiles (Ø 5 cm Plexiglass sampling core).

2.3. Water column nutrient and chl a samples

To determine chlorophyll *a* (chl *a)* concentrations in the water column, NISKIN bottles were closed 3 m below the water surface, at the deep chlorophyll maximum (observed from CTD casts), and 5 m above the seafloor. Water samples were vacuum filtered over GF/F filters, and flash-frozen in liquid nitrogen before storage at −80 °C. In the laboratory, photosynthetic pigments were extracted from the filters using a 90% acetone dilution (Wright, 1991), and quantified through high performance liquid chromatography (HPLC; Zapata et al., 2000). Only chl *a* concentrations are discussed in this work. From the sea floor NISKIN samples, subsamples for DIC and nutrients were taken to characterize bottom water concentrations.

2.4. Subsample processing

Porewater nutrients were extracted from the sediment subsamples using rhizon samplers (0.15 μm pore size, Rhizosphere Research Products) at 1 cm depth intervals for the first 8 cm, and then at 2 cm intervals down to 12 cm. The rhizons were inserted into the sediment core through pre-drilled holes in the core wall, and a maximum of 4 mL of porewater was extracted from each interval by connecting a 5 mL syringe and creating a vacuum (Seeberg-Elverfeldt et al., 2005; Dickens et al., 2007; Shotbolt, 2010). Porewater nutrient samples were stored and analysed in the same way as the water nutrient samples.

Sediment grain size was determined by laser diffraction on freeze-dried and sieved (<1 mm) sediment samples in a Malvern Mastersizer 2000 (McCave et al., 1986). Water content was determined as the volume of water removed by freeze drying wet sediment samples. The sediment density was determined by measuring the water displacement

of a given weight of dried sediment. Sediment porosity was determined from water content and solid phase density measurements, accounting for the salt content of the pore water. The Corg/N ratio was calculated from Corg. and N concentrations, determined using an Interscience Flash 2000 organic element analyser. Sediment permeability was determined using a permeameter (Buchanan, 1984).

Clark-type O_2 micro-electrodes (50 μm tip diameter, Unisense) were used to measure oxygen-depth profiles in the sediment (Revsbech, 1989). In each sediment core, up to three replicate profiles were taken from different areas of the sediment. For each profile, readings were taken at 100 μm intervals, starting 2000 μm (2 mm) above the sediment-water interface (water aerated to 100% O_2 saturation before the experiment) down to the depth in the sediment at which all oxygen was depleted, the maximum oxygen penetration depth (OPD). A two-point calibration was conducted prior to measurements using 100 and 0% oxygen saturated seawater to represent water column and anoxic O_2 concentrations, respectively. Note that profiles were only measured up to 1 mm for the coarse sandy station D.240.

2.5. Biogeochemical modelling

2.5.1. Model structure

Modelling of steady state sediment biogeochemistry was conducted with the OMEXDIA diagenetic modelling framework (Soetaert et al., 1996), extended to include simplified phosphorus dynamics (Ait Ballagh et al., 2020) in line with the model of Slomp et al. (1996a). This diagenetic model describes the dynamics of organic matter degradation on a 1D grid down to 100 cm deep, consisting of 100 layers, and with increasing layer thickness starting at 0.01 cm near the sediment water interface (SWI). Two classes of organic matter (detritus) with differing reactivity (fast decaying FDET, slow decaying SDET) are mineralized sequentially in oxic mineralization, followed by denitrification, and anoxic mineralization (Table 2). Consumption of oxygen and nitrate is explicitly modelled (Eqs. 1.1, 1.2), mineralization is limited by carbon availability (first order kinetics), and oxidant availability (Michaelis-Menten type kinetics), and inhibited by concentrations of inhibiting solutes. The anoxic mineralization with oxidants other than oxygen and nitrate (manganese oxides, iron oxides, sulfate, organic matter) are collected into one process in which so-called oxygen demand units (ODU's) are generated (Eq. 1.3). The reoxidation of these ODU's, as well as the nitrification are two additional processes that consume O_2 (Eqs. 1.4, 1.5). Phosphorus dynamics include the formation and release of Fe-bound phosphorus (FeP), as well as the formation and dissolution of Ca-bound P, apatite (CaP) (Ait Ballagh et al., 2020). Including the two classes of organic matter and dissolved organic carbon (DIC), this makes for 11 species, each defined in the 100 sediment layers.

State variables are transported in the sediment through advection, molecular diffusion (for solutes) and bioturbation (solids). The solute flux due to molecular diffusion and advection is described by Fick's first law (Fick, 1855),

$$J_D = \phi D_i \frac{\partial C}{\partial z} + \phi v C \quad (1)$$

where the effective diffusion coefficient is written as $D_i = D_0/\theta^2$, with D_0 the molecular diffusivity of the solute, $\theta^2 = 1–2$ ln (ϕ) the correction factor for sediment tortuosity (Boudreau, 1996), and ϕ the sediment porosity, which was kept constant with depth. Bioturbation is depth-dependent (z), and was set as a constant biodiffusivity value Db_0 in a surficial layer with thickness L_{mix}. Below this depth, bioturbation decreases rapidly to zero, determined by the attenuation coefficient for bioturbation (Db_{coeff}, Eq. (2)).

$$Db_z = Db_0 e^{-\frac{(z - L_{mix})}{Db_{coeff}}} \quad (2)$$

Deposition fluxes and bottom water concentrations were imposed for the upper boundaries of solid and liquid substances respectively, while a zero-gradient was assumed at the lower boundary.

Boundary conditions and parameters for the model obtained from measurements were temperature, salinity, solute bottom water concentrations (NO_3^-, NH_4^+, PO_4^{3-}, O_2, DIC), and the sediment porosity ϕ. The model was implemented in R (R Core Team, 2020), the transport of simulated species was calculated using the R-package ReacTran (Soetaert and Meysman, 2012), while steady state was estimated using the R-package rootSolve (Soetaert, 2009). Molecular diffusion coefficients were calculated using R-package marelac (Soetaert and Petzoldt, 2018).

2.5.2. Model fitting

Fitting of the diagenetic model to the data was done in two steps. Using the measured DIC flux as the upper boundary carbon input flux, profiles were first manually fitted. Measured fluxes of O_2, and porewater profiles of NH_4^+, NO_3^-, and PO_4^{3-} were approximated by manually tweaking a limited set of parameters (see Table 3). The degradation rate of slow degrading material (*rSlow*), and the biodiffusivity constant *Db*

Table 2
Diagenetic reactions used in OMEXDIA. x denotes the molar C:P ratio, y the molar N:P ratio in organic matter per mole of phosphorus (for Redfield Stoichiometry, x = 106, y = 16).

Process	Reaction	
Oxic mineralization	$(CH_2O)x\ (NH_3)y\ (H_3PO_4) + xO_2 \rightarrow xCO_2 + yNH_3 + H_3PO_4 + xH_2O$	(1.1)
Denitrification	$(CH_2O)x\ (NH_3)y\ (H_3PO_4) + 0.8 \times HNO_3 \rightarrow xCO_2 + yNH_3 + 0.4 \times N_2 + H_3PO_4 + 1.4 \times H_2O$	(1.2)
Anoxic mineralization	$(CH_2O)x\ (NH_3)y\ (H_3PO_4)$ + an oxidant → $xCO_2 + yNH_3 + H_3PO_4$ + xODU + xH_2O	(1.3)
Nitrification	$NH_3 + 2O_2 \rightarrow HNO_3 + H_2O$	(1.4)
ODU oxidation	ODU + O_2 → an oxidant	(1.5)

Table 3
Model parameters, and values.

Parameter	Parameter meaning	Unit	Type	Value (range)
Φ	Porosity	–	Measured	0.45–0.71
wSed	Solid phase advection rate	cm yr^{-1}	Fixed	0.0365
pFast	Fast degrading fraction organic matter	–	Fixed	0.95
pSlow	Slow degrading fraction organic matter	–	Fixed	0.05
rFast	Decay rate FDET	d^{-1}	Fixed	0.05
rSlow	Decay rate SDET	d^{-1}	Fitted	$0.11{\cdot}10^{-3}$ - $0.53{\cdot}10^{-3}$
Db	Biodiffusivity coefficient	$cm^2\ d^{-1}$	Fitted	0.001–0.019
biotdepth	Mixed layer depth	cm	Fixed	2
rnit	Max. nitrification rate	d^{-1}	Fitted	2–34.7
rODUox	Max. ODU oxidation rate	d^{-1}	Fitted	4–70
ksO2oduox	Half saturation, O_2 in ODU oxidation	mmol $O_2\ m^{-3}$	Fitted	1–8
ksNO3denit	Half saturation, NO_3 in denitrification	mmol $NO_3\ m^{-3}$	Fitted	15–100
kinO2denit	Half saturation, O_2 inhibition of denitrification	mmol $O_2\ m^{-3}$	Fitted	20–100
kinNO3anox	Half saturation, NO_3 inhibition anoxic mineralization	mmol $NO_3\ m^{-3}$	Fitted	1–8
kinO2anox	Half saturation, O_2 inhibition anoxic mineralization	mmol $O_2\ m^{-3}$	Fitted	35–97
rCaPprod	Rate of CaP production	d^{-1}	Fitted	0–0.06
rCaPdiss	Rate of CaP dissolution	d^{-1}	Fitted	0–0.001
rFePadsorp	Rate of FeP adsorption	d^{-1}	Fitted	0.1–2.7
rFePdesorp	Rate of FeP desorption	d^{-1}	Fitted	0–0.0066

were constrained by fitting the NH_4^+, and O_2 profiles. Parameters affecting the NO_3^- and NH_4^+ profiles were then tuned, starting with the nitrification rate *rnit*, followed by the denitrification constants *ksNO3denit*, and *kinO2denit*. The shape of the oxygen profiles further constrained the oxidation rate of oxygen demanding units (ODU's), and reaction constants for anoxic mineralization *kinO2anox* and *kinNO3anox*. In the last manual fitting step, the modelled phosphate profiles were adjusted by changing the parameters for the processes affecting FeP and CaP. This could be done in the last step, as the phosphate dynamics do not impact the other model constituents. The manual fitting was followed by a constrained parameter fitting using an optimization algorithm. In this second step, the fitted parameters were allowed to vary in a range ±10 % around the manually fitted parameters. Also the DIC fluxes were refitted within a narrow range (0.98–1.02 of measured value), to allow freedom to the fitting algorithm. A random-based minimization algorithm (Price, 1977) implemented in the R package FME (Soetaert and Petzoldt, 2010) was used. This algorithm pseudo-randomly samples the parameter space, until the parameter set was found which returned the minimal model cost, the latter defined as the sum of variable costs (modelled - measured values), scaled using the mean - standard deviation relation determined for each nutrient.

2.5.3. Post-processing

Based on the model results, the total stock of particulate organic carbon (POC) in the top 0.1 m of the sediment was calculated as the sum of both reactive classes of carbon (FDET, SDET), and the fraction of nonreactive carbon. The former was estimated from the model results, the latter was derived by subtracting the reactive carbon from the measured sediment organic carbon content C_{org} (top 2 cm, Table 4). Net P release/scavenging rates were calculated for the oxic and anoxic zones in the sediment by summing release processes (FeP and CaP release) and subtracting the scavenging processes (FeP and CaP formation). Trends between the model output (process rates, carbon stock), model parameters; and the sampling depth, and latitude were explored through Pearson's correlation (*r*) tests with 9 degrees of freedom, with a significance level (*p*-value) of 0.05. Analyses were performed in R (R Core Team, 2020).

3. Results

3.1. Description of the sampling sites

The sampling stations differed in their sediment characteristics (Table 4). The sediment median grain size ranged between 25 ± 1 μm and 217 ± 2 μm, the differences mostly due to the relative contributions of fine (125–250 μm) and very fine sand (63–125 μm), and the silt content (<63 μm). Deeper stations (C.450, F.640, F.695, F.770) had the smallest median grain size (25 ± 1 to 70 ± 8 μm), due to a high proportion of silt (40 ± 4 to 88 ± 2%), the lowest permeability ($1.0{\cdot}10^{-16}$ ± 0 m^2 to $1.6{\cdot}10^{-14} \pm 0.40{\cdot}10^{-14}$), and the highest organic carbon (0.45 ± 0.06 to 1.12 ± 0.03%) and nitrogen content (0.05 ± 0.01 to 0.14 ± 0.01%). The shallowest station (D.240), and stations C.380 and C.545 had sediments with the greatest median grain size (192 ± 1 to 217 ± 2 μm) and fine sand content (48 ± 2 to 63 ± 2%), and of the studied locations were the only to classify as permeable, instead of cohesive sediments (according the threshold of 10^{-12} m^2 of Huettel et al. (2014); $1.0{\cdot}10^{-12} \pm 0.09{\cdot}10^{-12}$ to $7.4{\cdot}10^{-12} \pm 0.42{\cdot}10^{-12}$ m^2). Additionally, these stations had lower contents of organic carbon (0.06 ± 0.01 to 0.23 ± 0.02%) and total nitrogen (0.01 ± 0 to 0.03 ± 0%). The stations on either slope of the Dogger Bank (O.100 - O.190, and C.300) contained the highest fraction of very fine sands (36 ± 1 to 55 ± 1%), intermediate contents of organic carbon and nitrogen (resp. 0.17 ± 0.01 to 0.28 ± 0.09% and 0.02 ± 0 to 0.03 ± 0.01%), and an intermediate permeability relative to the other zones ($3.1{\cdot}10^{-14} \pm 2.58{\cdot}10^{-14}$ to $7.2{\cdot}10^{-13} \pm 6.02{\cdot}10^{-13}$ m^2).

Along the transect, bottom water concentrations of NO_3^- (1.5 mmol m^{-3} at O.100 to 8.8 mmol m^{-3} at F.770) and PO_4^{3-} (0.6 mmol m^{-3} at O.100 to 3.1 mmol m^{-3} at F.770) increased northward (Table 1). Values for bottom water NH_4^+ (7.4 ± 8.6 mmol m^{-3}) and O_2 (253.9 ± 27.1 mmol m^{-3}) displayed no systematic pattern.

Water column chl *a* concentration was highest in the DCM of station O.100 (11.1 μg L^{-1}, Fig. 2). Other stations with noticeably higher chl *a* concentrations in the DCM compared to bottom or surface values were stations C.300, C.545, and F.640 (resp. 2.0, 1.2, and 3.9 μg L^{-1}). Chl *a* values near the surface and the bottom were generally similar for a given location, with highest concentrations measured at O.100 (2.2–2.6 μg L^{-1} surface – bottom resp.). Values decreased towards the Dogger Bank (0.4–0.6 μg L^{-1}), and from then on ranged between 0.2 and 0.4 μg L^{-1} for surface concentrations, and 0.1–0.3 μg L^{-1} for bottom water concentrations, increasing northward. No clear patterns were found in the sediment surface chl *a* concentrations (μg chl *a* per g dry sediment), which ranged from 2.9 ± 2.6 μg g^{-1} at O.100 to 0.3 ± 0.3 μg g^{-1} at C.545 (Fig. 2).

3.2. Sediment profiles

In general, gradients in nutrient concentrations were only pronounced within the top 3–6 cm of the sediment. At greater depths, solute concentrations stayed relatively constant (Fig. 3). Only ammonium profiles of D.240, F.640 and F.770 suggest a further build-up below the sampling horizon of 12 cm. Deep porewater concentrations (>8 cm) of NH_4^+ were lowest in the Oyster Grounds (O.135: 44.5 ± 15.1 mmol m^{-3}) and the Dogger Bank (53.4 ± 6.9 mmol m^{-3}), and were highest in the central North Sea (C.380: 64.1 ± 8.6 mmol m^{-3}), and Devils Hole (C.450, 87.6 ± 7.6 mmol m^{-3}). Values then decreased again in the Fladen Ground stations (F.695: NH_4^+ = 49.2 ± 21.0 mmol m^{-3}), with the exception of F.770 (NH_4^+ = 62.4 ± 21.0 mmol m^{-3}), where two out of three profiles did show a further increase in concentrations below 6 cm (Fig. 3). Phosphate profiles displayed a similar trend as the ammonium profiles. Deep concentrations of PO_4^{3-} were highest in the central North

Table 4
Sediment parameters (mean ± sd) for each sampling station.

Parameter Unit	MGS (μm)	Fines (%)	vFines (%)	Silt (%)	Permeability (m^2)	Porosity (−)	Chl *a* (μg g^{-1})	C_{org} (%)	N_{tot} (%)	C/N (mol mol^{-1}) >
O.100	82 ± 9	17 ± 1	51 ± 12	32 ± 11	$3.14{\cdot}10^{-14} \pm 2.58{\cdot}10^{-14}$	0.57 ± 0.08	3.62 ± 0.93	0.28 ± 0.09	0.03 ± 0.01	10.20 ± 0.24
O.135	103 ± 3	29 ± 2	55 ± 1	16 ± 0	$5.72{\cdot}10^{-14} \pm 3.28{\cdot}10^{-14}$	0.46 ± 0.01	0.84 ± 0.27	0.17 ± 0.01	0.02 ± 0.00	8.91 ± 0.25
O.190	125 ± 5	47 ± 3	36 ± 1	15 ± 5	$6.18{\cdot}10^{-14} \pm 0.33{\cdot}10^{-14}$	0.45 ± 0.01	1.28 ± 0.25	0.20 ± 0.07	0.03 ± 0.01	8.57 ± 0.54
D.240	217 ± 2	63 ± 2	4 ± 0	0 ± 0	$7.39{\cdot}10^{-12} \pm 0.42{\cdot}10^{-12}$	0.39 ± 0.01	0.99 ± 0.01	0.06 ± 0.01	0.01 ± 0.00	6.66 ± 1.41
C.300	113 ± 1	39 ± 0	47 ± 1	14 ± 1	$7.24{\cdot}10^{-13} \pm 6.02{\cdot}10^{-13}$	0.48 ± 0.00	3.35 ± 1.16	0.27 ± 0.01	0.03 ± 0.00	9.37 ± 0.65
C.380	212 ± 2	48 ± 2	6 ± 1	9 ± 2	$1.01{\cdot}10^{-12} \pm 0.08{\cdot}10^{-12}$	0.43 ± 0.02	0.59 ± 0.28	0.22 ± 0.02	0.03 ± 0.00	9.13 ± 0.17
C.450	70 ± 8	19 ± 4	35 ± 1	45 ± 5	$1.71{\cdot}10^{-14} \pm 0.34{\cdot}10^{-14}$	0.57 ± 0.03	2.85 ± 1.56	0.67 ± 0.02	0.09 ± 0.00	9.03 ± 0.07
C.545	192 ± 1	59 ± 1	8 ± 0	9 ± 1	$4.86{\cdot}10^{-12} \pm 1.67{\cdot}10^{-12}$	0.46 ± 0.01	0.35 ± 0.01	0.23 ± 0.02	0.03 ± 0.00	8.51 ± 0.24
F.640	25 ± 1	1 ± 1	11 ± 1	88 ± 2	$5.11{\cdot}10^{-15} \pm 5.37{\cdot}10^{-15}$	0.71 ± 0.02	2.26 ± 0.53	1.12 ± 0.03	0.14 ± 0.01	9.04 ± 0.11
F.695	57 ± 52	24 ± 1	16 ± 1	40 ± 4	$1.00{\cdot}10^{-16} \pm 0$	0.49 ± 0.08	0.78 ± 0.24	0.45 ± 0.06	0.05 ± 0.01	10.13 ± 1.21
F.770	55 ± 1	10 ± 0	34 ± 1	56 ± 1	$1.59{\cdot}10^{-14} \pm 0.40{\cdot}10^{-14}$	0.61 ± 0.05	0.73 ± 0.53	0.65 ± 0.02	0.08 ± 0.00	9.35 ± 0.09

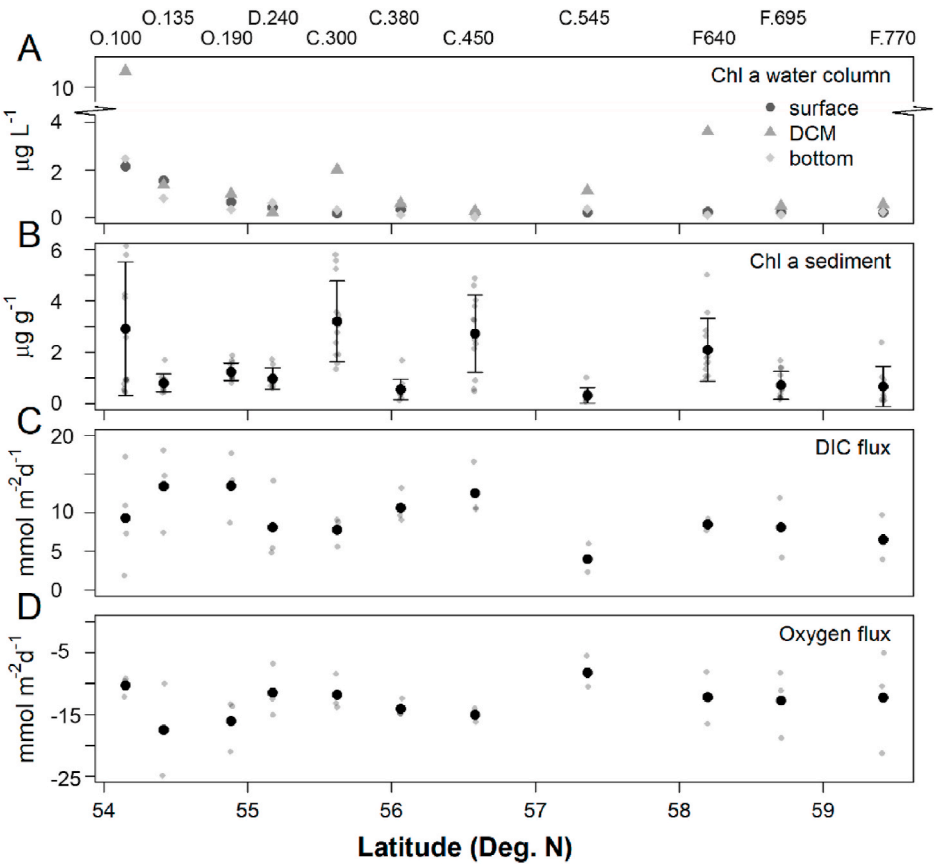

Fig. 2. (A) Chlorophyll *a* concentrations in the water column near the surface, the bottom, and at the deep chlorophyll maximum (DCM, µg Chl *a* L^{-1}), (B) Chlorophyll *a* in the upper 2 cm of the sediment (µg Chl *a* g^{-1}), (C) the DIC flux (mmol m^{-2} d^{-1}), and (D) oxygen fluxes (mmol m^{-2} d^{-1}) measured along the transect. Black points in B, C, and D represent the means of the measured values (gray points), error bars (in B) the standard deviation.

Sea (e.g. C.380: 19.2 ± 5.6 mmol m^{-3}), and in station F.770 in the Fladen Grounds (20.1 ± 10.8 mmol m^{-3}). Deep PO_4^{3-} concentrations in the Oyster Grounds (O.135: 11.1 ± 11.4 mmol m^{-3}), and the Fladen Grounds were lower (F.695: 9.0 ± 2.9 mmol m^{-3}). Nitrate profiles did not display consistent features in the first 5 stations starting from the coast, and concentrations remained low all over the sediment (range of 1.6 ± 1.4 to 3.4 ± 6.2 mmol m^{-3}). From C.380 northwards however, nitrate concentrations clearly decreased just below the sediment water interface. These were also the locations where the oxygen penetration depths were markedly higher and ranged from 6.8 ± 2.0 mm to 7.9 ± 0.4 mm, as opposed to lowest penetration depths in the Oyster Grounds (2.4 ± 0.9 mm to 5.9 ± 2.4 mm), and intermediate values in the central North Sea (3.2 ± 0.2 mm to 4.4 ± 0.4 mm).

3.3. Sediment fluxes

The measured oxygen influxes varied from −8.24 ± 2.52 mmol m^{-2} d^{-1} at C.545, to −16.03 ± 4.35 and −17.52 ± 7.45 mmol m^{-2} d^{-1} at O.135 and O.190 (Table 5). Note that negative fluxes represent an uptake in the sediment, positive fluxes exit the sediment. The DIC effluxes were also lowest for C.545 (3.98 ± 1.85 mmol m^{-2} d^{-1}), and highest at O.190 (13.52 ± 4.54 mmol m^{-2} d^{-1}). Oxygen and DIC fluxes were significantly correlated ($r = -0.47$, $p = 0.005$), and the DIC release significantly decreased with latitude ($r = -0.35$, $p = 0.045$), which was not the case for the oxygen fluxes ($r = -0.13$, $p = 0.46$) (Fig. 2).

The measured nutrient fluxes displayed a high heterogeneity within sampling replicates, with replicate cores of the same stations sometimes resulting in in- and effluxes for the same solute (Table 5). In general, more than 40% of regressions of nutrient concentrations over time were not significant, so that nutrient fluxes were assumed 0 mmol m^{-2} d^{-1}. Highest ammonium release was measured on the Dogger Bank (0.85 ± 1.29 mmol m^{-2} d^{-1}), and the bordering stations (O.190, C.300), whereas NH_4^+ uptake by the sediment was measured at O.135, and in the northern third of the transect (sts. C.545, F.640, F.770). Besides O.100, where nitrate uptake was measured (−0.21 ± 0.55 mmol m^{-2} d^{-1}), NO_3^- efflux varied between 0 mmol m^{-2} d^{-1} at C.300 to 0.56 ± 0.96 mmol m^{-2} d^{-1} at F.640. Phosphate exchange was significantly correlated with the station depth ($r = 0.67$, $p = 0.025$); in the southern half of the transect, PO_4^{3-} uptake occurred in O.100, and the Dogger Bank, whereas in the northern part exclusively PO_4^{3-} release occurred (with highest efflux measured at Devils Hole, 0.08 ± 0.09 mmol m^{-2} d^{-1}).

3.4. Modelling results

3.4.1. Model parametrization

The combination of the heuristic (manual) profile fitting step and the optimization algorithm produced parameter sets which adequately describe the measured porewater solute profiles (Table 3, Fig. 3). Ammonium and oxygen profiles were shaped initially by a combination of the bioturbation rate *Db*, and the decay rate of the slow degrading organic matter *rSlow*. Decreasing the bioturbation rate reduced the build-up of NH_4^+ (and PO_4^{3-}) with depth, increased the oxygen penetration depth, and changed the shape of the NO_3^- profile (deepening the NO_3^- peak). While the degradation rate of slow degrading organic matter also impacted the deep NH_4^+ concentrations, it had the largest effect on the *shape* of the NH_4^+ profile, with lower degradation rates causing a more gradual build-up with sediment depth. Derived bioturbation rates ranged from 0.001 cm^2 d^{-1} at O.135 to 0.019 cm^2 d^{-1} at C.545, and degradation rates of slow degrading carbon ranged from $1 \cdot 10^{-4}$ d^{-1} at D.240 to $5.3 \cdot 10^{-4}$ d^{-1} at C.545. The nitrification rate was the parameter

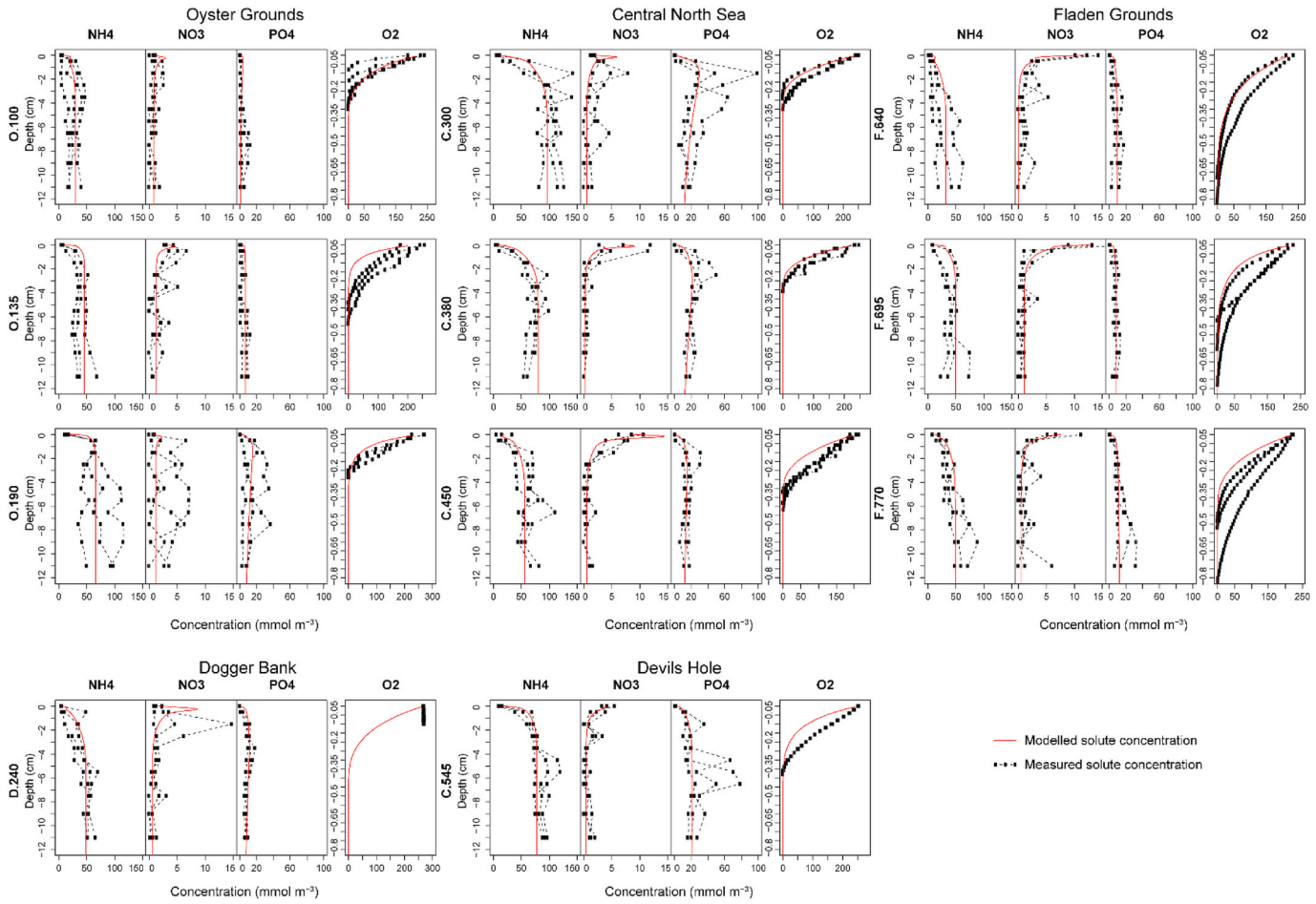

Fig. 3. Measured porewater solute profiles (dotted lines) and model fits (red lines) for NH_4^+, NO_3^-, PO_4^{3-} and O_2. (For interpretation of the references to color in this figure legend, the reader is referred to the Web version of this article.)

Table 5
Measured solute fluxes of ammonium (NH_4^+), nitrate (NO_3^-), phosphate (PO_4^{3-}), oxygen (O_2), and dissolved inorganic carbon (DIC) in mmol m^{-2} d^{-1}, with negative values indicating a flux into the sediment, positive values a flux out of the sediment.

Station	NH_4^+	NO_3^-	PO_4^{3-}	DIC	O_2
O.100	0.04 ± 0.77	−0.21 ± 0.55	−0.04 ± 0.05	9.3 ± 6.46	−10.27 ± 1.32
O.135	−0.22 ± 0.38	0.35 ± 0.31	0.09 ± 0.08	13.43 ± 5.45	−17.52 ± 7.45
O.190	0.73 ± 0.64	0.26 ± 0.03	0.00 ± 0.00	13.52 ± 4.54	−16.03 ± 4.35
D.240	0.85 ± 1.29	0.15 ± 0.26	−0.01 ± 0.12	8.11 ± 5.2	−11.45 ± 4.25
C.300	0.84 ± 0.24	0.00 ± 0.00	0.00 ± 0.00	7.82 ± 1.93	−11.82 ± 2.94
C.380	0.71 ± 0.44	0.43 ± 0.74	0.00 ± 0.00	10.64 ± 2.21	−14.11 ± 1.43
C.450	0.68 ± 0.38	0.43 ± 0.37	0.08 ± 0.09	12.56 ± 3.52	−15.02 ± 1.08
C.545	−0.10 ± 0.16	0.33 ± 0.00	0.01 ± 0.00	3.98 ± 1.85	−8.24 ± 2.52
F.640	0.00 ± 0.00	0.56 ± 0.96	0.04 ± 0.04	8.48 ± 0.74	−12.15 ± 4.22
F.695	0.45 ± 0.43	0.24 ± 0.41	0.03 ± 0.03	8.12 ± 3.85	−12.77 ± 5.41
F.770	0.00 ± 0.00	0.25 ± 0.00	0.04 ± 0.07	6.54 ± 2.92	−12.27 ± 8.23

used to reconcile the nitrate and ammonium profiles. Increasing the nitrification rate slightly decreased the build-up of NH_4^+, and increased concentrations of NO_3^-, typically producing a nitrate concentration peak within the oxic zone. Parameters concerning the oxidation of ODU's (*rODUox*, *ksO2oduox*), and oxygen inhibition parameters for denitrification and anoxic mineralization (*kinO2denit*, *kinO2anox*) were adjusted where necessary to better fit the nitrate profiles. In some cases (Fig. 3: O.100, C.300), the model was unable to fit a NO_3^- profile without a subsurface peak between 0 and 1 cm, without simultaneously compromising the NH_4^+ concentration.

After fitting the O_2, NH_4^+, and NO_3^- profiles, phosphate concentrations were generally already in the correct order of magnitude, and the parameters describing the FeP and CaP dynamics were mostly needed to further define the shape of the profiles. Phosphate profiles with a visible subsurface peak, such as D.240, C.300, C.380, and C.545, could only be generated by the formation of CaP (*CaPprod*), thus causing a decrease of PO_4^{3-} with depth. The FeP formation rate (*FePads*) proved a necessary parameter to regulate the phosphate concentrations in the oxic region. This was often coupled to FeP desorption (*FePdes*) in deeper layers, as this shuttle of P was needed to supply free phosphate to be used in CaP production in deeper layers (Table 6).

Modelled fluxes for DIC and O_2 were positively correlated with their measured counterparts (r of 0.97, and 0.90 respectively, $p < 0.001$). For NO_3^-, NH_4^+, and PO_4^{3-} no significant correlation between measured and

Table 6
Model derived mineralization rates (mmol C m^{-2} d^{-1}), nitrification (mmol O_2 m^{-2} d^{-1}), relative contributions of each mineralization process to the total mineralization, net P removal and release in the oxic and anoxic sediment layers (μmol m^{-2} d^{-1}), the proportion of incoming nitrogen removed from the sediment, and the stock of carbon in the top 0.1 m of sediment (moles m^{-2}).

	Mineralization Rates (mmol m^{-2} d^{-1})					Relative proportions (%)		
	Oxic	Denitrification	Anoxic	Total	Nitrification	Oxic	Denitrification	Anoxic
O.100	7.02	0.29	2	9.3	0.91	75.4	3.1	21.5
O.135	12.14	0.1	1.19	13.43	0.53	90.4	0.7	8.9
O.190	10.66	0.04	2.83	13.52	0.3	78.8	0.3	20.9
D.240	6.42	0.25	1.44	8.11	0.84	79.2	3.1	17.7
C.300	4.61	0.18	3.03	7.82	0.96	58.9	2.4	38.7
C.380	6.95	0.48	3.21	10.64	1.25	65.3	4.5	30.2
C.450	9.01	0.18	3.38	12.56	0.56	71.7	1.4	26.9
C.545	2.28	0.32	1.37	3.98	1.17	57.4	8.1	34.5
F.640	6.21	1.06	1.21	8.48	1.12	73.2	12.5	14.3
F.695	6.36	0.46	1.29	8.12	0.31	78.4	5.7	15.9
F.770	4.35	0.54	1.65	6.54	1.12	66.4	8.3	25.2

	Net. free P scavenging (−) or release (+) (μmol P m^{-2} d^{-1})		**Removal proportions (% of mineralized)**		**C stock in top 0.1 m of sediment (moles m^{-2})**	
	Oxic sed.	**Anoxic sed.**	**Nitrogen**	**Phosphorus**	**POC**	**DIC**
O.100	−0.16	0.04	16	25	25.41	0.3
O.135	−0.08	−0.04	4	9	4.31	0.28
O.190	−0.12	0.09	2	1	8.38	0.29
D.240	−0.01	−0.01	17	1	2.47	0.31
C.300	−0.09	0.06	12	6	14.70	0.35
C.380	−0.06	0.05	24	0	12.02	0.35
C.450	−0.05	0.07	7	0	67.95	0.31
C.545	−0.04	0.03	43	1	18.95	0.31
F.640	−0.02	−0.01	66	4	143.51	0.29
F.695	−0.01	0.00	30	2	33.99	0.28
F.770	−0.02	0.01	44	0	73.67	0.29

modelled fluxes could be achieved (NO_3^-: $r = -0.44$, $p = 0.18$; NH_4^+: $r = 0.25$, $p = 0.46$; PO_4^{3-}: $r = 0.4$, $p = 0.22$).

3.4.2. Model output

The total carbon mineralization rates showed a decreasing trend northward ($r = -0.55$, $p = 0.079$; Table 6). Most of the carbon mineralization was due to oxic processes (57–90%) (Fig. 4). The lowest contribution of oxic mineralization to total carbon mineralization was found in the central North Sea stations, where its contribution ranged between 57 and 72% (C.300, C.380, C.450, C.545). Here, the contribution of anoxic mineralization was maximal and reached 30–39%. The relative importance of oxic mineralization was negatively correlated to both the bioturbation rates (*Db*, oxic: $r. = -0.79$, $p = 0.004$; anoxic: $r = 0.58$, $p = 0.07$), and the nitrification rates (*rnit*, oxic: $r = -0.64$, $p = 0.03$; anoxic: $r. = 0.43$, $p = 0.17$). Nitrification (range: 0.30–1.25 mmol O_2 m^{-2} d^{-1}) contributed on average 10% (±7) to the oxygen consumption budget, with a clear outlier at C.545 (25%, Table 6). No clear latitudinal patterns in nitrification were observed.

Denitrification had a relatively smaller contribution to total mineralization in most southern stations up to Devils hole (C.450, 0–5%), but was responsible for up to 6–13% of the total carbon mineralization in the most Northern stations (C.545 and Fladen Grounds), leading to a significant latitudinal increase ($r = 0.69$, $p = 0.018$). As a result of increased denitrification rates, sediments in this zone removed the

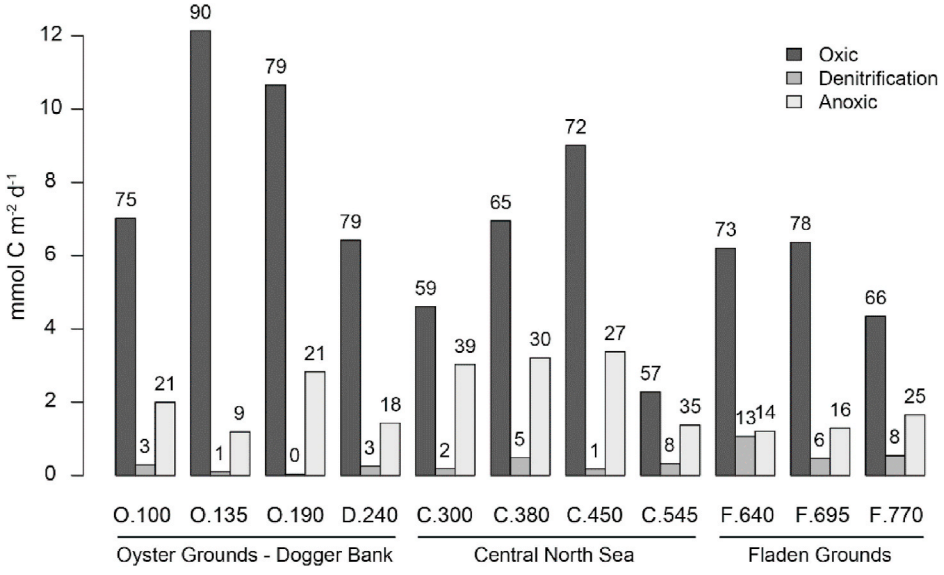

Fig. 4. Model-derived C mineralization rates for oxic mineralization, denitrification, and anoxic mineralization in mmol m^{-2} d^{-1} (bars), and what they represent as a percentage of the total mineralization at each site (numbers above the bars).

highest amount of reactive nitrogen from the sediment: denitrification removed 30–66% of all organic N mineralized in the Fladen Grounds, vs. 2–16% in the Oyster Grounds (Table 6). In contrast, phosphate removal rates were highest at O.100 and O.135 (resp. 25 and 9% of all produced P). In these stations, high P removal rates were found in the oxic zone (resp. 0.16 and 0.12 μmol P m^{-2} d^{-1}), also characteristic for O.190 and C.300 (resp. 0.12 and 0.09 μmol P m^{-2} d^{-1}). For the remainder of the stations, P removal was between 0 and 6%.

Stocks of particulate organic carbon (POC) in the upper 10 cm ranged from 2.47 mol m^{-2} at C.300 to 143.51 mol m^{-2} at the Fladen Grounds (Table 6). POC values were significantly correlated to water depth ($r = 0.71$, $p < 0.015$) as well as the silt content of the sediment ($r = 0.96$, $p < 0.001$).

4. Discussion

In this study, we set out to characterize the response of organic matter mineralization processes to spring bloom deposition in several distinct regions of the North Sea. The research cruise was planned to take place after the spring bloom, and the chl *a* values measured in the water column along the transect indicate that this was indeed the case (Fig. 2). The water column was highly stratified, with a prominent deep chlorophyll maximum (DCM) present for most of the stations (observed from CTD casts). Surface and bottom water chl *a* values (resp. 1.45 ± 0.75 and 1.21 ± 1.13 μg L^{-1}) for the Oyster Grounds correspond to those found in this region by Boon et al. (1998), whereas the values found in the Fladen Grounds (0.22 ± 0.01 μg L^{-1}) are similar to the post-bloom values reported in Eiane and Ohman (2004) in the same region. Naturally, the spring bloom is a heterogeneous event throughout the sampled region (Desmit et al., 2019; van Leeuwen et al., 2015); and there were 12 days between the first, and last station sampled (Table 1). For these reasons, it is likely that an unknown amount of variability seen in the data will reflect this difference in timing.

Despite this temporal variation and the heterogeneity of sediments (Table 4) sampled over a considerable distance (670 km), total mineralization rates differed with a factor 3.4 at most (3.98–13.52 mmol C m^{-2} d^{-1}), with measured DIC fluxes ranging between 2 and 18 mmol m^{-2} d^{-1} (Table 5). Previously reported values of DIC fluxes in the southern North Sea (the area up to the Fladen Grounds, 2–29 mmol m^{-2} d^{-1}), and northern North Sea (Fladen Grounds, 0–6 mmol m^{-2} d^{-1}), showed a slightly wider range (values measured in September, Brenner et al., 2016). Our measured oxygen consumption rates (5–25 mmol O_2 m^{-2} d^{-1}) also compared well to previously measured values in spring/early summer available for the Oyster Grounds and Dogger Bank (4–14 mmol O_2 m^{-2} d^{-1}, Osinga et al. (1996); Raaphorst et al. (1990); Wilde et al. (1984)), the German Bight (15.5–25.1 mmol O_2 m^{-2} d^{-1} (Oehler et al., 2015)), the Central North Sea area (7–18 mmol O_2 m^{-2} d^{-1}, Upton et al. (1993)), and the Fladen Grounds (1–7 mmol O_2 m^{-2} d^{-1}, de Wilde et al. (1986)).

The measurements and modelling results suggest that the response to carbon deposition was broadly similar for all studied sites: a mostly oxic mineralization of organic matter, resulting in a low sedimentary nutrient build-up. However, there were differences in the biogeochemical signatures between regions with different sediment characteristics. The sediments along the southern part of the transect displayed coarser particle size and greater permeability from the Oyster Ground stations towards the Dogger Bank (Table 4). Mineralization in this zone was predominantly coupled to oxygen consumption (75–90%, Fig. 4), with a small contribution of denitrification (0–3%) to total mineralization. The sediments in the Central North Sea were more permeable and relatively coarse grained, except for Devils Hole sediments which were characterized by high silt contents and a low permeability. Anoxic mineralization was more important in this central region (27–39%), while denitrification contributed more to total mineralization (1–8%). Lastly, the Fladen Grounds had the finest sediments, with an intermediary importance of oxic mineralization (66–78%) and the highest proportion of mineralization as denitrification (6–13%).

4.1. Rapid, oxic mineralization

While a surficial, mostly oxic mineralization of organic matter has been observed for several regions in the southeast of the North Sea (Upton et al., 1993; Lohse et al., 1995; Raaphorst and Malschaert, 1996), our results indicate that this occurs throughout large parts of the North Sea. The high contribution of oxic mineralization can be deduced from the shape of the solute profiles close to the sediment water interface (Fig. 3). In nearly all locations, the gradients in nutrient concentrations were established in the upper 4–6 cm, exhibiting a rather constant concentration below that depth. This shape was observed even where solute concentrations were higher, such as the central North Sea stations northwest of the Dogger Bank (Fig. 3). Free nutrients are produced where organic matter mineralization takes place. When most of the organic matter mineralization occurs in oxic conditions (i.e. near the sediment-water interface), the bulk of the free nutrients will be produced near the sediment water interface as well. As a result, solute profiles rapidly reach constant concentrations, as mineralization in deeper layers will not contribute much to the pool of nutrients. In our study, such profiles were observed in the Oyster grounds and Central North Sea. Only on the Dogger Bank, and in two stations in the Fladen Grounds, F.640 and F.770, solute profiles exhibited a more gradual build-up that seemingly continued beyond 12 cm depth, suggesting that organic matter degradation was shifted away from the sediment surface there. The degree to which degradation occurs near to the surface was partly caused by the bioturbation rates in the model, which were lowest on the Oyster Grounds (0.001 cm^2 d^{-1}), and highest in the Central North Sea (0.019 cm^2 d^{-1}). Bioturbation mixes fresh organic matter deeper into the sediment, which decreases the substrate for mineralization near the surface, while increasing the organic matter content in deeper (sub- and anoxic) sediment layers.

The stock of particulate organic carbon in the upper 10 cm correlated strongly with the silt content in the sediment (Fig. 5). Whereas this relation was not unexpected (Wilson et al., 2018; Serpetti et al., 2012), it confirmed the Fladen Grounds and the Oyster Grounds as areas of increased carbon burial (Van Raaphorst et al., 1998), while most of the North Sea is bereft of any considerable carbon burial (De Haas et al., 1997). Higher values of the observed POC stock in the Fladen Grounds of 34–144 mol m^{-2}, and in Devils Hole: 68 mol m^{-2} exceed average values for surrounding sediments of the Central (37 mol m^{-2}), and Northern North Sea (43 mol m^{-2}) respectively (Legge et al., 2020), and resemble more the POC stocks calculated for the Norwegian Trench (54–120 mol m^{-2}, Legge et al., 2020).

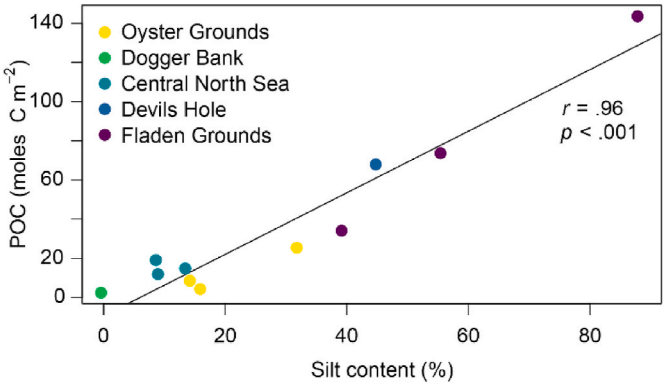

Fig. 5. Particulate organic carbon (POC, moles m^{-2}) in the top 0.1 m of the sediment, as a function of the silt content per station.

4.2. Large-scale patterns

Several trends were found along the transect. Total mineralization rates, as well as the contribution of oxic mineralization decreased from south to north, whereas the importance of denitrification increased (Fig. 4). The decreasing trend in total mineralization has previously been noted in the North Sea, and was attributed to lower temperatures in deeper waters, changes in sediment granulometry, and a weakened coupling to pelagic production (Brenner et al., 2016). While we found no clear latitudinal pattern in sedimentary nor water column chl *a* concentrations, our data do show correspondence between DCM and top sediment chl *a* concentrations in multiple locations (O.100, C.300, F.640; Fig. 2), signaling a direct input of fresh material to sediments in most regions.

4.2.1. Increasing denitrification northward

The increasing proportion of organic matter mineralized via denitrification, appeared to be driven predominantly by increasing bottom water nitrate concentrations towards the north (Table 1). Overall, modelled denitrification rates (0.03–0.85 mmol N m^{-2} d^{-1}) compared well to measured denitrification rates in the North Sea, which range from 0 to 0.50 mmol N m^{-2} d^{-1} in the Oyster Grounds and the Dogger Bank (Lohse et al., 1995; Neubacher et al., 2011). Rosales Villa et al. (2019) measured a denitrification rate of 0.19 mmol N m^{-2} d^{-1} near the Fladen Grounds (in August), which is low compared to our modelled rates for this region, but *in situ* NO_3^- bottom water concentrations were also 30–60% lower than ours in the cited study.

On the Oyster Grounds, all NO_3^- produced from nitrification was subsequently denitrified (Fig. 6 A). In the Dogger Bank and central North Sea sediments, nitrification rates were slightly higher (with the exception of Devils Hole), and exceeded the NO_3^- demand of denitrification (Fig. 6 A). The significant negative correlation between the nitrification rates and the proportion of oxic mineralization indicates that nitrification in the Dogger Bank and the central North Sea sediments competes for oxygen with organic matter mineralization processes, with this decrease in available oxygen resulting in a higher proportion of anoxic mineralization of organic matter.

In contrast, the higher denitrification rates on the Fladen Grounds were only sustained for ~25% by nitrate produced from nitrification, with most of the NO_3^- provided by the overlying water (Fig. 6 A). This intake of nitrate from the bottom water can be seen in the NO_3^- profiles in the Fladen Grounds, which have highest values near the sediment water interface, and a steep decline below where it is consumed (Fig. 3). Elevated bottom water NO_3^- concentrations in the Fladen Grounds, up to ten times those on the Oyster Grounds, are most likely explained by the inflow of nutrient rich Atlantic water (Holt et al., 2012; Vermaat et al., 2008). These bottom water concentrations thus explain these profiles, and the NO_3^- uptake in the sediment (Table 1). A result of this increased denitrification towards the North, was that in the Oyster Grounds only 2–26% of all mineralized N was removed from the sediment through N_2 production, whereas in the Fladen Grounds this increased to 30–66% (Fig. 6 B). This shows that the deep regions of the North Sea are potentially considerable sinks of nitrogen, driven by bottom water nitrate concentrations.

It should be noted that the absence of additional relations between denitrification rates and other determining factors (e.g. carbon flux, C/N ratio, OPD) could point to the fact that we could not distinguish between so-called canonical denitrification (as used in the current model;

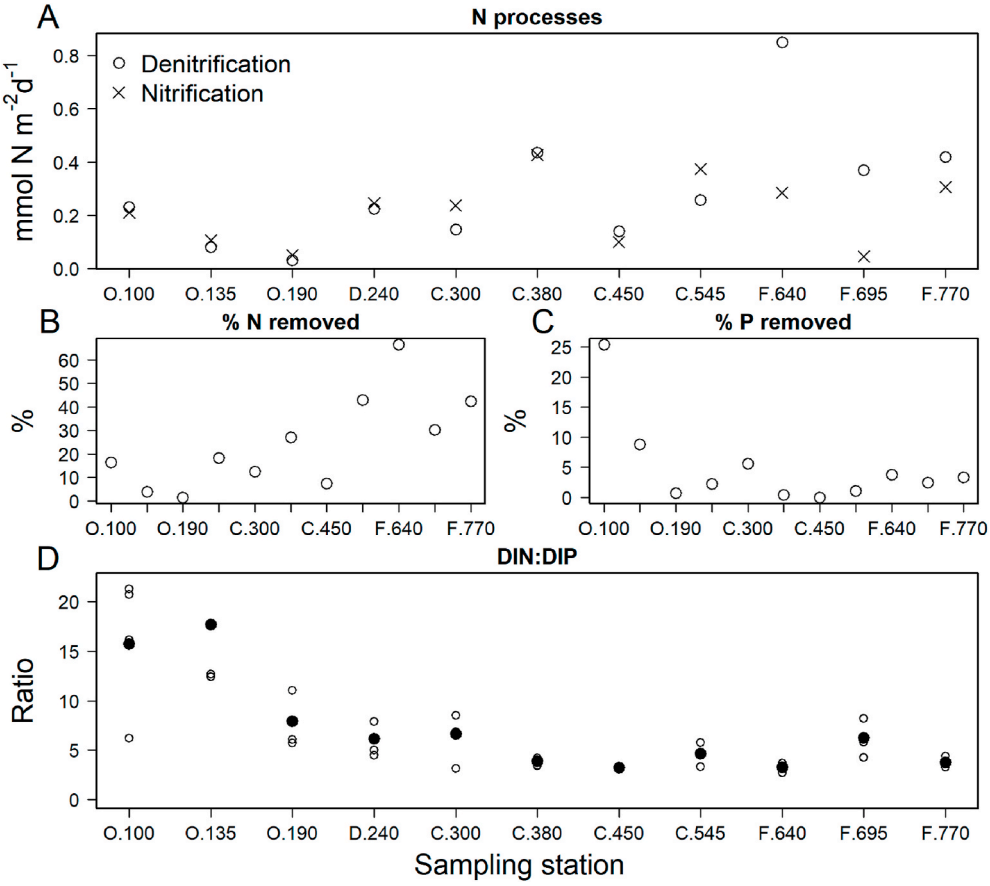

Fig. 6. (A) Nitrification and denitrification (mmol N m^{-2} d^{-1}) for each station; (B) net nitrogen removed as a % of N mineralized; (C) net % of mineralized phosphorus buried or removed from the sediment; (D) The DIN:DIP ratio in the sediment (from 2 cm downwards, black dots = average, empty dots = replicate values).

Brandes and Devol, 2002), and anammox (anaerobic ammonium oxidation). Both processes consume NH_4^+, and produce N_2, but different drivers influence the occurrence of annamox and canonical denitrification. Anammox can be of considerable importance in hemipelagic sediments, and may account for up to 25% of N_2 production on continental shelf sediments (Dale et al., 2011). The relative importance of anammox over denitrification has been linked to increasing depth, changes to organic matter quantity and quality, as well as nitrite availability and faunal ventilation activity (Dalsgaard et al., 2005; Dale et al., 2011). To separate both with certainty, high resolution nitrite profiles and fluxes, as well as N_2 fluxes are needed. That being said, a previous study on nitrogen cycling that included samples in the Fladen Grounds (in August) reported only denitrification as a cause of N_2 production, and not anammox (Rosales Villa et al., 2019).

4.2.2. Decreasing DIN:DIP ratios northward

Differences in N cycling along the transect caused changes in the sedimentary concentration of dissolved inorganic nitrogen (NOx + NHx, DIN), relative to dissolved inorganic phosphorus (PO_4^{3-}, DIP), but differences in P-cycling between the different stations altered this ratio just as well (Fig. 6 C). The DIN:DIP ratio gives an indication of the efficiency with which N compared to P is retained (or conversely, removed) in the sediment as mineralization proceeds. Higher and lower DIN:DIP ratios in deep sediments indicate more efficient removal of P or N respectively. For the deeper layers (2–12 cm) the DIN:DIP ratio was highest in O.100 and O.135 (16 ± 11 and 18 ± 16), but for the other stations values were much lower, ranging between 3 ± 1 (C.450) to 8 ± 4 (O.190), often indicating a depletion of DIN relative to DIP in the sediments (Fig. 6 D). Whereas denitrification decreases DIN concentrations in the sediment relative to DIP, the processes that affect DIP are more complex.

The P-cycle in marine sediments is strongly driven by the deposition of organic matter, and the redox conditions in the sediment. In oxic conditions, iron is present in solid form as oxides, and this binds phosphate to form FeP complexes (Slomp et al., 1996a,b). As the FeP is mixed below the oxic zone, the Fe-oxides will reductively dissolve through dissimilatory Fe-reduction, or sulphide induced dissolution (an end product of anoxic sulfate reduction). This resulting PO_4^{3-} release from FeP dissolution increases phosphate concentrations in deeper sediment layers (Mortimer, 1942; Ingall and Jahnke, 1994; Colman and Holland, 2000; Slomp, 2012). The sequestration of P in the oxic zone, and release of P in the anoxic zone has been called the P-shuttle mechanism, and causes a preferential build-up of phosphate over ammonium at depth into the sediment. In addition, in deeper sediment layers, calcium phosphate minerals can be formed (authigenic CaP), with or without FeP as an intermediate (Slomp, 2011). This causes removal of dissolved P and burial of solid-phase P, which constitutes the main P-sink in the sediment. The removal of dissolved P to the solid phase is evident in PO_4^{3-} profiles as a gradual decrease of PO_4^{3-} with increasing sediment depth in the anoxic zone, causing inorganic phosphorus to be depleted compared to ammonium at depth. It should be noted that, as we did not measure neither FeP nor CaP, our model could not distinguish between P shuttling and removal by either Fe- or Ca-related processes. However, the net P removal to the solid phase could be deduced from the decrease of phosphate with sediment depth.

The highest removal of P in the oxic zone occurred in O.100 and O.135, and this was not (O.135), or only partially (O.100) linked to release in the anoxic zone (Table 6). On the Oyster Grounds and Dogger Bank sediments in general, surficial (0–2 cm) and deep PO_4^{3-} concentrations were lowest relative to DIN (DIN:DIP surface: 24 ± 23; below 2 cm: 16 and 18, Fig. 6 D).

In the central North Sea sediments, the model also indicated significant removal of phosphate in the oxic zone, leading to surface N:P values of 16 ± 11. However, in the Central North Sea – Fladen Ground stations deep DIN:DIP ratios varied from 3 to 9, as in these station more solid P was released back to free PO_4^{3-} in the anoxic zone (Table 6). This shuttle caused build-up of PO_4^{3-} deeper in the sediment which, in combination with slightly higher denitrification rates, led to low DIN:DIP ratios (3–6 average). In the Central North Sea and the Fladen Ground sediments, modelled PO_4^{3-} processes showed less formation of solid P. The amount of buried P was thus much higher in the Oyster Grounds (specifically O.100, and O.135), with more constant values for the rest of the transect (Fig. 6 C).

Because of the combination of increasing nitrogen removal and decreasing DIP removal, the DIN:DIP ratio in the deep porewater was highest near the coast, and decreased further offshore (Fig. 6 D). Interestingly, this pattern is consistent with the decreasing DIN:DIP ratio in the water column with distance from the coast that has been observed since the 1990's (Burson et al., 2016). De-eutrophication efforts (OSPAR, 1988), have decreased P inputs to coastal waters of the North Sea by 50–70%, but reduced the N load by only 20–30% (Lenhart et al., 2010; Passy et al., 2013). As a result of this, DIN:DIP ratios in the water column have been observed to be elevated above Redfield (N:P of 16:1, Redfield (1960)) from the coast, up to the eastern slope of the Dogger Bank in April (Burson et al., 2016). In summary, the pattern of decreasing DIN:DIP ratios we observed is explained on one hand by increased P burial, and a link to similar DIN:DIP dynamics in the water column closer to shore, and on the other hand by increasing N removal by denitrification towards the north.

5. Conclusions

The combination of field measurements and diagenetic modelling showed rapid mineralization of fresh organic matter in the sediments of a region of the North Sea extending from 100 km from the Dutch coast up to the Fladen Grounds in the northern part of the North Sea. This resulted in an overall low nutrient build-up, despite significant differences in sediment characteristics and environmental conditions. The similarity of the mineralization response characterizes the study area as a zone of fast nutrient recycling, where fresh organic material is recycled to nutrients that are available to the water column within weeks, or a few months after deposition. Total mineralization decreased with increasing latitude, revealing subtle differences in mineralization processes, such as increased removal of nitrogen and decreased removal of P towards the north. 1-D diagenetic modelling, combined with measured solute fluxes, and porewater nutrient profiles proved a robust tool in deriving mineralization rates. The results of this research expedition contribute valuable knowledge about the biogeochemical functioning of several understudied regions of the North Sea.

Declaration of competing interest

The authors declare that they have no known competing financial interests or personal relationships that could have appeared to influence the work reported in this paper.

Acknowledgements

E.D.B. is a doctoral research fellow funded by the Belgian Science Policy Office (BELSPO) BELSPO, contract BR/154/A1/FaCE-It. U.B. is a postdoctoral research fellow at Research Foundation - Flanders (FWO, Belgium) (Grant 1201720N). We acknowledge the funding of the Netherlands Organisation for Scientific Research NWO and Royal Netherlands Institute for Sea Research NIOZ in organising the Netherlands Initiative Changing Oceans NICO expedition in 2018. We thank laboratory staff: Jan Peene, Jurian Brasser, Peter van Breugel and Yvonne van der Maas, the captain and crew of the RV Pelagia, chief scientist Rob Witbaard, as well as students who assisted during sampling: Sterre Witte, Nina Fieten. Lastly, we thank three anonymous reviewers for their valuable comments on the manuscript.

References

Ahmerkamp, S., Marchant, H.K., Peng, C., Probandt, D., Littmann, S., Kuypers, M.M.M., Holtappels, M., 2020. The effect of sediment grain properties and porewater flow on microbial abundance and respiration in permeable sediments. Sci. Rep. 10, 1–12. https://doi.org/10.1038/s41598-020-60557-7.

Ait Ballagh, F.E., Rabouille, C., Andrieux-Loyer, F., Soetaert, K., Elkalay, K., Khalil, K., 2020. Spatio-temporal dynamics of sedimentary phosphorus along two temperate eutrophic estuaries: a data-modelling approach. Continent. Shelf Res. 193, 104037. https://doi.org/10.1016/j.csr.2019.104037.

Boon, A.R., Duineveld, G.C.A., Berghuis, E.M., Van Der Weele, J.A., 1998. Relationships between benthic activity and the annual phytopigment cycle in near-bottom water and sediments in the southern North sea. Estuar. Coast Shelf Sci. 46, 1–13. https://doi.org/10.1006/ecss.1997.0264.

Boudreau, B.P., 2000. The mathematics of early diagenesis: from worms to waves. Rev. Geophys. 38, 389–416. https://doi.org/10.1029/2000RG000081.

Boudreau, B.P., 1996. The diffusive tortuosity of fine-grained unlithified sediments. Geochem. Cosmochim. Acta 60, 3139–3142. https://doi.org/10.1016/0016-7037(96)00158-5.

Braeckman, U., Foshtomi, M.Y., Van Gansbeke, D., Meysman, F., Soetaert, K., Vincx, M., Vanaverbeke, J., 2014. Variable importance of macrofaunal functional biodiversity for biogeochemical cycling in temperate coastal sediments. Ecosystems 17, 720–737. https://doi.org/10.1007/s10021-014-9755-7.

Brenner, H., Braeckman, U., Le Guitton, M., Meysman, F.J.R., 2016. The impact of sedimentary alkalinity release on the water column CO2 system in the North Sea. Biogeosciences 13, 841–863. https://doi.org/10.5194/bg-13-841-2016.

Buchanan, J.B., 1984. Sediment Analysis, 2nd Ed, Methods for the Study of Marine Benthos, second ed. Blackwell Scientific Publications, Oxford. https://doi.org/10.1002/9781118542392.

Burson, A., Stomp, M., Akil, L., Brussaard, C.P.D., Huisman, J., 2016. Unbalanced reduction of nutrient loads has created an offshore gradient from phosphorus to nitrogen limitation in the North Sea. Limnol. Oceanogr. 61, 869–888. https://doi.org/10.1002/lno.10257.

Canfield, D., Jørgensen, B., Fossing, H., Glud, R., Gundersen, J., Ramsing, N., Thamdrup, B., Hansen, J., Nielsen, L., Hall, P.O., 1993. Pathways of organic carbon oxidation in three continental margin sediments. Mar. Geol. 113, 27–40. https://doi.org/10.1016/0025-3227(93)90147-N.

Capuzzo, E., Lynam, C.P., Barry, J., Stephens, D., Forster, R.M., Greenwood, N., McQuatters-Gollop, A., Silva, T., van Leeuwen, S.M., Engelhard, G.H., 2018. A decline in primary production in the North Sea over 25 years, associated with reductions in zooplankton abundance and fish stock recruitment. Global Change Biol. 24, e352–e364. https://doi.org/10.1111/gcb.13916.

Cardenas, M.B., Cook, P.L.M., Jiang, H., Traykovski, P., 2008. Constraining denitrification in permeable wave-influenced marine sediment using linked hydrodynamic and biogeochemical modeling. Earth Planet Sci. Lett. 275, 127–137. https://doi.org/10.1016/j.epsl.2008.08.016.

Colman, A.S., Holland, H.D., 2000. The global diagenetic flux of phosphorus from marine sediments to the oceans: redox sensitivity and the control of atmospheric oxygen levels. Marine Authigenesis: from Global to Microbial. SEPM (Society for Sedimentary Geology), pp. 53–75. https://doi.org/10.2110/pec.00.66.0053.

Dauwe, B., Middelburg, J.J., 1998. Amino acids and hexosamines as indicators of organic matter degradation state in North Sea sediments. Limnol. Oceanogr. 43, 782–798. https://doi.org/10.4319/lo.1998.43.5.0782.

De Haas, H., Boer, W., Van Weering, T.C.E., 1997. Recent sedimentation and organic carbon burial in a shelf sea: the North Sea. Mar. Geol. 144, 131–146. https://doi.org/10.1016/S0025-3227(97)00082-0.

de Wilde, P.A.W.J., Berghuis, E.M., Kok, A., 1986. Biomass and activity of benthic fauna on the fladen ground (northern North Sea). NJSR (Neth. J. Sea Res.) 20, 313–323. https://doi.org/10.1016/0077-7579(86)90053-0.

Desmit, X., Nohe, A., Borges, A.V., Prins, T., De Cauwer, K., Lagring, R., Van der Zande, D., Sabbe, K., 2019. Changes in chlorophyll concentration and phenology in the North Sea in relation to de-eutrophication and sea surface warming. Limnol. Oceanogr. 1–20. https://doi.org/10.1002/lno.11351.

Dickens, G.R., Koelling, M., Smith, D.C., Schnieders, L., 2007. Rhizon sampling of pore waters on scientific drilling expeditions: an example from the IODP expedition 302, Arctic Coring Expedition (ACEX). Sci. Drill. 22–25. https://doi.org/10.2204/iodp.sd.4.08.2007.

Eiane, K., Ohman, M.D., 2004. Stage-specific mortality of Calanus finmarchicus, Pseudocalanus elongatus and oithona similis on fladen ground, North Sea, during a spring bloom. Mar. Ecol. Prog. Ser. 268, 183–193. https://doi.org/10.3354/meps268183.

Galloway, J.N., Dentener, F.J., Capone, D.G., Boyer, E.W., Howarth, R.W., Seitzinger, S. P., Asner, G.P., Cleveland, C.C., Green, P.A., Holland, E.A., Karl, D.M., Michaels, A. F., Porter, J.H., Townsend, A.R., Vorosmarty, C.J., 2004. Nitrogen cycles: past, present, and future. Biogeochemistry 70, 153–226. https://doi.org/10.1007/s10533-004-0370-0.

Gieskes, W.W.C., Kraay, G.W., 1984. Phytoplankton, its pigments, and primary production at a central north sea station in May, July and September 1981. NJSR (Neth. J. Sea Res.) 18, 51–70. https://doi.org/10.1016/0077-7579(84)90024-3.

Glud, R.N., 2008. Oxygen dynamics of marine sediments. Mar. Biol. Res. 4, 243–289. https://doi.org/10.1080/17451000801888726.

Greenwood, N., Parker, E.R., Fernand, L., Sivyer, D.B., Weston, K., Painting, S.J., Kröger, S., Forster, R.M., Lees, H.E., Mills, D.K., Laane, R.W.P.M., 2010. Detection of low bottom water oxygen concentrations in the North Sea; Implications for monitoring and assessment of ecosystem health. Biogeosciences 7, 1357–1373. https://doi.org/10.5194/bg-7-1357-2010.

Holt, J., Butenschön, M., Wakelin, S.L., Artioli, Y., Allen, J.I., 2012. Oceanic controls on the primary production of the northwest European continental shelf: model experiments under recent past conditions and a potential future scenario. Biogeosciences 9, 97–117. https://doi.org/10.5194/bg-9-97-2012.

Holt, J., Schrum, C., Cannaby, H., Daewel, U., Allen, I., Artioli, Y., Bopp, L., Butenschon, M., Fach, B.A., Harle, J., Pushpadas, D., Salihoglu, B., Wakelin, S., 2016. Potential impacts of climate change on the primary production of regional seas: a comparative analysis of five European seas. Prog. Oceanogr. 140, 91–115. https://doi.org/10.1016/j.pocean.2015.11.004.

Huettel, M., Berg, P., Kostka, J.E., 2014. Benthic exchange and biogeochemical cycling in permeable sediments. Ann. Rev. Mar. Sci. 6, 23–51. https://doi.org/10.1146/annurev-marine-051413-012706.

Ingall, E., Jahnke, R., 1994. Evidence for enhanced phosphorus regeneration from marine sediments overlain by oxygen depleted waters. Geochem. Cosmochim. Acta 58, 2571–2575. https://doi.org/10.1016/0016-7037(94)90033-7.

Jodo, M., Kawamoto, K., Tochimoto, M., Coverly, S.C., 1992. Determination of nutrients in seawater by segmented-flow analysis with higher analysis rate and reduced interference on ammonia. J. Automat. Chem. 14, 163–167. https://doi.org/10.1155/S1463924692000300.

Joint, I., Pomroy, A., 1993. Phytoplankton biomass and production in the southern North Sea. Mar. Ecol. Prog. Ser. 99, 169–182. https://doi.org/10.3354/meps099169.

Jørgensen, B.B., 1982. Mineralization of organic matter in the sea bed—the role of sulphate reduction. Nature 296, 643–645. https://doi.org/10.1038/296643a0.

Legge, O., Johnson, M., Hicks, N., Jickells, T., Diesing, M., Aldridge, J., Andrews, J., Artioli, Y., Bakker, D.C.E., Burrows, M.T., Carr, N., Cripps, G., Felgate, S.L., Fernand, L., Greenwood, N., Hartman, S., Kröger, S., Lessin, G., Mahaffey, C., Mayor, D.J., Parker, R., Queirós, A.M., Shutler, J.D., Silva, T., Stahl, H., Tinker, J., Underwood, G.J.C., Van Der Molen, J., Wakelin, S., Weston, K., Williamson, P., 2020. Carbon on the northwest European shelf: contemporary budget and future influences. Front. Mar. Sci. 7 https://doi.org/10.3389/fmars.2020.00143.

Lenhart, H.J., Mills, D.K., Baretta-Bekker, H., van Leeuwen, S.M., Molen, J. van der, Baretta, J.W., Blaas, M., Desmit, X., Kühn, W., Lacroix, G., Los, H.J., Ménesguen, A., Neves, R., Proctor, R., Ruardij, P., Skogen, M.D., Vanhoutte-Brunier, A., Villars, M. T., Wakelin, S.L., 2010. Predicting the consequences of nutrient reduction on the eutrophication status of the North Sea. J. Mar. Syst. 81, 148–170. https://doi.org/10.1016/j.jmarsys.2009.12.014.

Lohse, L., Malschaert, J.F.P., Slomp, C.P., Helder, W., van Raaphorst, W., 1995. Sediment-water fluxes of inorganic nitrogen compounds along the transport route of organic matter in the North Sea. Ophelia 41, 173–197. https://doi.org/10.1080/00785236.1995.10422043.

McCave, I.N., Bryant, R.J., Cook, H.F., Coughanowr, C.A., 1986. Evaluation of a laser-diffraction-size analyzer for use with natural sediments. J. Sediment. Res. 56, 561–564. https://doi.org/10.1306/212f89cc-2b24-11d7-8648000102c1865d.

Middelburg, J.J., Soetaert, K., Herman, P.M.J., 1997. Empirical relationships for use in global diagenetic models. Deep-Sea Res. Part I Oceanogr. Res. Pap. 44, 327–344. https://doi.org/10.1016/S0967-0637(96)00101-X.

Middelburg, J.J., Soetaert, K., Herman, P.M.J., Heip, C.H.R., 1996. Denitrification in marine sediments: a model study. Global Biogeochem. Cycles 10, 661–673. https://doi.org/10.1029/96GB02562.

Mortimer, C.H., 1942. The exchange of dissolved substances between mud and water in lakes. J. Ecol. 30, 147. https://doi.org/10.2307/2256691.

Neubacher, E.C., Parker, R.E., Trimmer, M., 2011. Short-term hypoxia alters the balance of the nitrogen cycle in coastal sediments. Limnol. Oceanogr. 56, 651–665. https://doi.org/10.4319/lo.2011.56.2.0651.

Oehler, T., Martinez, R., Schückel, U., Winter, C., Kröncke, I., Schlüter, M., 2015. Seasonal and spatial variations of benthic oxygen and nitrogen fluxes in the Helgoland Mud Area (southern North Sea). Continent. Shelf Res. 106, 118–129. https://doi.org/10.1016/j.csr.2015.06.009.

Osinga, R., Kop, A.J., Duineveld, G.C.A., Prins, R.A., Van Duyl, F.C., 1996. Benthic mineralization rates at two locations in the southern North Sea. J. Sea Res. 36, 181–191. https://doi.org/10.1016/s1385-1101(96)90788-1.

Ospar, 1988. PARCOM Recommendation 88/2: on the Reduction in Nutrients to the Paris Convention Area. Paris Comission.

Passy, P., Gypens, N., Billen, G., Garnier, J., Thieu, V., Rousseau, V., Callens, J., Parent, J.-Y., Lancelot, C., 2013. A model reconstruction of riverine nutrient fluxes and eutrophication in the Belgian Coastal Zone since 1984. J. Mar. Syst. 128, 106–122. https://doi.org/10.1016/j.jmarsys.2013.05.005.

Price, W.L., 1977. A controlled random search procedure for global optimisation. Comput. J. 20, 367–370. https://doi.org/10.1093/comjnl/20.4.367.

Probandt, D., Knittel, K., Tegetmeyer, H.E., Ahmerkamp, S., Holtappels, M., Amann, R., 2017. Permeability shapes bacterial communities in sublittoral surface sediments. Environ. Microbiol. 19, 1584–1599. https://doi.org/10.1111/1462-2920.13676.

R Core Team, 2020. R: A Language and Environment for Statistical Computing.

Raaphorst, W. Van, Kloosterhuis, H.T., Cramer, A., Bakker, K.J.M., 1990. Nutrient early diagenesis in the sandy sediments of the dogger bank area, north sea: pore water results. NJSR (Neth. J. Sea Res.) 26, 25–52. https://doi.org/10.1016/0077-7579(90)90054-K.

Raaphorst, W. Van, Malschaert, J.F.P., 1996. Ammonium adsorption in superficial North Sea sediments. Continent. Shelf Res. 16, 1415–1435. https://doi.org/10.1016/0278-4343(95)00081-X.

Redfield, A.C., 1960. The biological control of chemical factors in the environment. Sci. Prog. 11, 150–170.

Reid, P.C., Lancelot, C., Gieskes, W.W.C., Hagmeier, E., Weichart, G., 1990. Phytoplankton of the north Sea and its dynamics: a review. NJSR (Neth. J. Sea Res.) 26, 295–331. https://doi.org/10.1016/0077-7579(90)90094-W.

Revsbech, N.P., 1989. An oxygen microsensor with a guard cathode. Limnol. Oceanogr. 34, 474–478. https://doi.org/10.4319/lo.1989.34.2.0474.
Rosales Villa, A.R., Jickells, T.D., Sivyer, D.B., Parker, E.R., Thamdrup, B., 2019. Benthic nitrogen cycling in the north sea. Continent. Shelf Res. 185, 31–36. https://doi.org/10.1016/j.csr.2018.05.005.
Seeberg-Elverfeldt, J., Schluter, M., Feseker, T., Kolling, M., 2005. Rhizon sampling of porewaters near the sediment-water interface of aquatic systems. Limnol. Oceanogr. 3, 361–371. https://doi.org/10.1016/S0012-821x(02)01064-6. Pii S0012-821x(02)01064-6.
Seitzinger, S., Harrison, J.A., Böhlke, J.K., Bouwman, A.F., Lowrance, R., Peterson, B., Tobias, C., Van Drecht, G., 2006. Denitrification across landscapes and waterscapes: a synthesis. Ecol. Appl. 16, 2064–2090. https://doi.org/10.1890/1051-0761(2006)016[2064:DALAWA]2.0.CO;2.
Serpetti, N., Heath, M., Rose, M., Witte, U., 2012. High resolution mapping of sediment organic matter from acoustic reflectance data. Hydrobiologia 680, 265–284. https://doi.org/10.1007/s10750-011-0937-4.
Shotbolt, L., 2010. Pore water sampling from lake and estuary sediments using Rhizon samplers. J. Paleolimnol. 44, 695–700. https://doi.org/10.1007/s10933-008-9301-8.
Slomp, C.P., 2011. Phosphorus cycling in the estuarine and coastal zones. In: Treatise on Estuarine and Coastal Science. Elsevier, pp. 201–229. https://doi.org/10.1016/B978-0-12-374711-2.00506-4.
Slomp, C.P., Epping, E.H.G., Helder, W., Raaphorst, W. Van, 1996a. A key role for iron-bound phosphorus in authigenic apatite formation in North Atlantic continental platform sediments. J. Mar. Res. 54, 1179–1205. https://doi.org/10.1357/0022240963213745.
Slomp, C.P., Van der Gaast, S.J., Van Raaphorst, W., 1996b. Phosphorus binding by poorly crystalline iron oxides in North Sea sediments. Mar. Chem. 52, 55–73. https://doi.org/10.1016/0304-4203(95)00078-X.
Soetaert, K., 2009. rootSolve: Nonlinear Root Finding, Equilibrium and Steady-State Analysis of Ordinary Differential Equations.
Soetaert, K., Herman, P.M.J., Middelburg, J.J., 1996. A model of early diagenetic processes from the shelf to abyssal depths. Geochem. Cosmochim. Acta 60, 1019–1040. https://doi.org/10.1016/0016-7037(96)00013-0.
Soetaert, K., Meysman, F., 2012. Reactive transport in aquatic ecosystems: rapid model prototyping in the open source software R. Environ. Model. Software 32, 49–60. https://doi.org/10.1016/j.envsoft.2011.08.011.
Soetaert, K., Middelburg, J.J., Herman, P.M.J., Buis, K., 2000. On the coupling of benthic and pelagic biogeochemical models. Earth Sci. Rev. 51, 173–201. https://doi.org/10.1016/S0012-8252(00)00004-0.
Soetaert, K., Petzoldt, T., 2018. Marelac. Tools for Aquatic Sciences.
Soetaert, K., Petzoldt, T., 2010. Inverse modelling, sensitivity and Monte Carlo analysis in R using PAckage FME. J. Stat. Software 33, 1–28. https://doi.org/10.18637/jss.v033.i03.
Stoll, M.H.C., Bakker, K., Nobbe, G.H., Haese, R.R., 2001. Continuous-flow analysis of dissolved inorganic carbon content in seawater. Anal. Chem. 73, 4111–4116. https://doi.org/10.1021/ac010303r.
Tijssen, S.B., Wetsteyn, F.J., 1984. Hydrographic observations near a subsurface drifter in the oyster ground, North sea. NJSR (Neth. J. Sea Res.) 18, 1–12. https://doi.org/10.1016/0077-7579(84)90021-8.
Upton, A.C., Nedwell, D.B., Parkes, R.J., Harvey, S.M., 1993. Seasonal benthic microbial activity in the southern North Sea - oxygen uptake and sulphate reduction. Mar. Ecol. Prog. Ser. 101, 273–282. https://doi.org/10.3354/meps101273.
Van Haren, H., Howarth, M.J., Jones, K., Ezzi, I., 2003. Autumnal reduction of stratification in the northern North Sea and its impact. Continent. Shelf Res. 23, 177–191. https://doi.org/10.1016/S0278-4343(02)00171-1.
van Leeuwen, S.M., Tett, P., Mills, D.K., van der Molen, J., 2015. Stratified and nonstratified areas in the North Sea: long-term variability and biological and policy implications. J. Geophys. Res. Ocean. 2121–2128. https://doi.org/10.1002/jgrc.20224.
van Leeuwen, S.M., van der Molen, J., Ruardij, P., Fernand, L., Jickells, T., 2013. Modelling the contribution of deep chlorophyll maxima to annual primary production in the North Sea. Biogeochemistry 113, 137–152. https://doi.org/10.1007/s10533-012-9704-5.
Van Raaphorst, W., Malschaert, H., Van Hanren, H., 1998. Tidal resuspension and deposition of particulate matter in the oyster grounds, North Sea. J. Mar. Res. 56, 257–291. https://doi.org/10.1357/002224098321836181.
Vermaat, J.E., McQuatters-Gollop, A., Eleveld, M.A., Gilbert, A.J., 2008. Past, present and future nutrient loads of the North Sea: causes and consequences. Estuar. Coast Shelf Sci. 80, 53–59. https://doi.org/10.1016/j.ecss.2008.07.005.
Weston, K., Fernand, L., Mills, D.K., Delahunty, R., Brown, J., 2005. Primary production in the deep chlorophyll maximum of the central North Sea. J. Plankton Res. 27, 909–922. https://doi.org/10.1093/plankt/fbi064.
Wilde, P.A.W.J.D., Berghuis, E.M., Kok, A., 1984. Structure and energy demand of the benthic community of the oyster ground, central North Sea. NJSR (Neth. J. Sea Res.) 18, 143–159. https://doi.org/10.1016/0077-7579(84)90029-2.
Wilson, R.J., Speirs, D.C., Sabatino, A., Heath, M.R., 2018. A synthetic map of the north-west European Shelf sedimentary environment for applications in marine science. Earth Syst. Sci. Data 10, 109–130. https://doi.org/10.5194/essd-10-109-2018.
Wollast, R., 1998. Evaluation and comparison of the global carbon cycle in the coastal zone and in the open ocean. In: Brink, K.H., Robinson, A. (Eds.), The Sea. John Wiley & Sons, Inc., Hoboken, New Jersey, pp. 213–252.
Wright, S.W., 1991. Improved HPLC method for the analysis of chlorophylls and carotenoids from marine phytoplankton. Mar. Ecol. Prog. Ser. 77, 183–196. https://doi.org/10.3354/meps077183.
Zapata, M., Rodriquez, F., Garrido, J., 2000. Separation of chlorophylls and carotenoids from marine phytoplankton: a new HPLC method using a. Mar. Ecol. Prog. Ser. 195, 29–45. https://doi.org/10.3354/meps195029.